Mechanistic Modeling of Protection Loss and Embrittlement Behavior of Cr-Coated Zirconium Alloy Cladding ATF under High-Temperature Steam Oxidation

Dongju Kim, Youho Lee *
Seoul National University, 1 Gwanak-ro, Gwanak-gu, Seoul 08826, Korea
**Corresponding author: leeyouho@snu.ac.kr*

Keywords : Cr-coated cladding, Steam oxidation, Protection loss, ATF, Embrittlement

1. Introduction

Chromium (Cr)-coated zirconium (Zr) alloy cladding is currently investigated as a primary Accident Tolerant Fuel (ATF) concept due to its superior oxidation resistance in high-temperature environments. However, prolonged exposure to steam at high temperatures (>1100 °C) results in a kinetic transition from protective parabolic growth to accelerated oxidation, a protection loss phase. This degradation is governed by the outward diffusion of Zr along the Cr grain boundaries (GBs), which facilitates the formation of continuous ZrO_2 pathways. These pathways compromise the integrity of the Cr_2O_3 scale, leading to rapid oxygen ingress and subsequent embrittlement of the underlying matrix.

Quantifying this protection loss and the resulting embrittlement is critical for evaluating the safety margins of coated claddings. Yet, most prior research [1, 2] has been limited to phenomenological observations, lacking integrated models that simulate the comprehensive degradation mechanism. To address this, this study aims at developing a mechanistic model to predict both the loss of coating protection and the subsequent embrittlement of the cladding under prolonged oxidation.

This study employed the Arc Ion Plating (AIP)-coated Zr-Nb alloy cladding subjected to high-temperature oxidation. Essential kinetic data for model development were derived through comprehensive microstructural analyses for post-oxidized specimens. Furthermore, the embrittlement induced by protection loss was experimentally evaluated via Post-Quench Ductility (PQD) tests following one-sided oxidation. The developed mechanistic model successfully predicted the decrease in ductile layer thickness and resulting embrittlement behavior, demonstrating it can serve as a reliable tool for predicting the coating failure and resulting embrittlement.

2. Modeling Framework

The mechanistic modeling framework for predicting the protection loss of Cr-coatings (Fig. 1) was derived and established in the previous study [3]. It integrates four interconnected sub-models to predict coating failure:

1. Transient Cr-coating thickness model: Tracks the continuous thinning of the coating driven by surface oxidation and interfacial Cr-Zr interdiffusion, defining the required depth of ZrO_2 path.

2. Cr-coating GB density model: Simulates the reduction in GB density due to recrystallization and grain growth, determining the number of available intergranular ZrO_2 paths.

3. ZrO_2 oxygen path in Cr-coating GB model: Models the kinetics of outward Zr diffusion along GBs and the subsequent growth and width of the intergranular ZrO_2 path.

4. Cr_2O_3 reduction and oxygen ingress model: Simulates the reduction of the protective Cr_2O_3 scale once the ZrO_2 path penetrates the coating, resulting in void formation and direct oxygen ingress into the substrate.

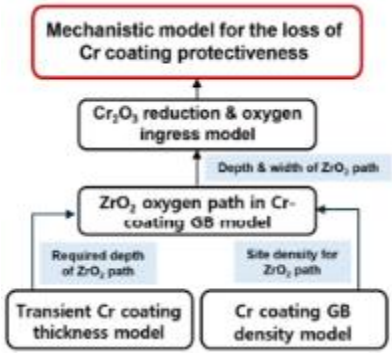

Fig. 1. Modeling framework for protection loss of Cr-coating.

3. Experimental Procedures

3.1 Cr-coated specimens

Cr-coatings were deposited onto Zr-Nb alloy cladding tubes (OD: 9.5 mm, ID: 8.36 mm) using a custom AIP facility at KEPCO Nuclear Fuel (KNF) [3]. Cross-sectional analysis verified the coating uniformity, yielding a thickness of 15.67 ± 0.64 μm (16 μm (AIP)).

3.2 High temperature oxidation and microstructure characterization for model development

Oxidation tests were performed using a Setaram THEMSYS Thermogravimetric Analyzer (TGA) [3]. Specimens were heated at 50 °C/min in a high-purity Helium (He) atmosphere to target temperatures of 1100–1300 °C, followed by steam injection (200 ml/min). To derive kinetic data, the oxidized samples underwent extensive microstructural characterization.

3.3 One-sided oxidation and PQD tests

To evaluate the cladding embrittlement following the loss of coating protection, one-sided high-temperature oxidation was conducted on 40 mm-long specimens, followed by direct quenching into boiling water and mechanical testing. To ensure exclusive outer-surface oxidation, the specimen ends were sealed using alumina plugs and a sodium silicate (Na_2SiO3)-based sealant. Experiments were performed in a simulated LOCA facility [4] at 1200 °C for durations of 3000–9000 s. Following the quenching, the oxidized specimens were sectioned into three 8 mm-long rings. Finally, Ring Compression Tests (RCTs) were carried out at 135 °C using an INSTRON 4702 machine to measure residual ductility.

4. Development of Sub-models and Integration

4.1 Transient Cr-coating thickness model

The transient coating thickness model predicts the remaining Cr-coating thickness by coupling two independent consumption mechanisms: surface oxidation and interfacial diffusion. For surface oxidation, the growth of the Cr_2O_3 scale follows parabolic kinetics prior to protection loss [5]. The resulting metal consumption is calculated by dividing the predicted oxide thickness by the Pilling–Bedworth ratio (PBR) of Cr_2O_3 (2.07).

Simultaneously, the diffusion-induced loss at the coating-substrate interface is simulated using a mechanistic Cr diffusion model based on the radial diffusion equation and the Zr-Cr phase diagram [6]. The total transient thickness is determined by subtracting these combined losses from the initial thickness. Validation against experimental data at 1100–1300 °C confirmed that the model predicts the coating thickness within a ±10% error margin (Fig. 2).

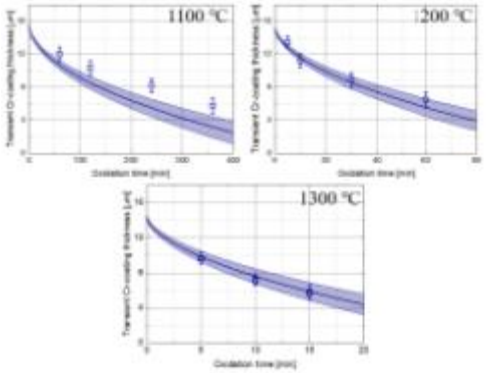

Fig. 2. Model-to-experiment comparison for transient Cr-coating thicknesses evolution at 1100–1300 °C.

4.2 Cr-coating GB density model

Since Zr diffusion is strictly intergranular, the GB density of the Cr-coating determines the number of potential failure sites. Experimental analysis revealed that the fine-grained microstructure undergoes rapid recrystallization and grain growth during the early stage of oxidation [3]. Notably, the GB density saturated within 5 minutes at 1200 °C, which is significantly shorter than the characteristic timescale for Zr diffusion to penetrate the coating (~75 minutes). This timescale disparity indicates that the diffusion site is established well before the onset of significant ZrO_2 path formation. Consequently, instead of modeling the time-dependent evolution, a material-specific constant value (Table I)—experimentally determined as the saturated linear GB density—was applied.

Table I: Measured saturated linear GB density [3]

Parameters (saturation)	Oxidation temperature [℃]		
	1100	1200	1300
Density [/μm]	0.096	0.108	0.096

4.3 ZrO_2 oxygen path in Cr-coating GB model

The formation of intergranular ZrO_2 paths is modeled based on the outward diffusion of Zr along Cr grain boundaries. The growth kinetics of the path depth ($\delta_{Zr\ depth}$) are governed by Fick's first law, assuming that the supplied Zr flux is instantaneously consumed to form the ZrO_2 phase. This leads to a parabolic growth law expressed as Eq. (1) where $K_{Zr\ depth}(T)$ is a temperature-dependent rate constant derived from an Arrhenius fit of experimental data (Eq. (2)). R and T represent gas constant and temperature, respectively.

$$\delta_{Zr\ depth}(t) = K_{Zr\ depth}(T)\sqrt{t} \quad (1)$$

$$K_{Zr\ depth}(T) = 486907\exp\left(-\frac{191080}{RT}\right)\ [\mu m/s^{0.5}] \quad (2)$$

Additionally, the width of the ZrO_2 path at the moment of protection loss, which determines the area for subsequent oxygen ingress, was determined empirically from microstructural observations and applied as a temperature-dependent parameter [3].

4.4 Cr_2O_3 reduction and oxygen ingress model

Upon the ZrO_2 path penetrating the coating, the protective Cr_2O_3 layer undergoes reduction, forming voids that facilitate steam entry (Fig. 3).

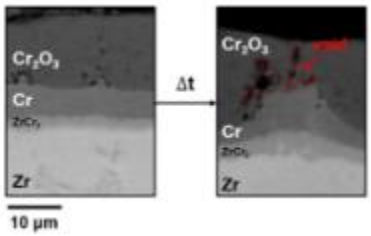

Fig. 3. SEM images of onset of reduction and protection loss stages with interconnected void.

The duration of this reduction phase ($t_{reduction}$) is modeled as a linear function of the Cr_2O_3 thickness at the onset of reduction, using empirically derived coefficients (Eqs. (3)-(4)).

$$t_{reduction} = K_{reduction}(T)\,\delta_{Cr_2O_3} \quad (3)$$

$$K_{reduction}(T) = 2.85110^{-4} \exp\left(\frac{20345}{T}\right) \ [s/\mu m] \quad (4)$$

Once the voids formed an interconnected path, oxygen diffusion into the Zr matrix is simulated. The oxygen flux through individual ZrO_2 paths ($J_{O,i}$) is calculated using Fick's law (Eq. (5)). Here, $\delta_{Cr,i}$ denotes the local Cr-coating thickness. $D_{O,\ path}$ represents the oxygen diffusivity within the oxide path, while $C_{O,path/steam}$ and $C_{O,path/Zr}$ define the boundary oxygen concentrations at the steam interface (accessible via interconnected voids) and the Zr matrix interface, respectively (Eqs. (6)-(8)).

$$J_{O,i} = D\frac{\partial C}{\partial r} = D_{O,\ path}\frac{C_{O,path/steam} - C_{O,path/Zr}}{\delta_{Cr,i}} \quad (5)$$

$$C_{O,path/steam} = 1.526\ [g/cm^3] \quad (6)$$

$$C_{O,path/Zr} = 1.5494 - 9.7\times 10^{-5}\ T\ [g/cm^3] \quad (7)$$

$$D_{O,path} = \begin{cases} \&0.127 \exp\left(-\frac{144396}{RT}\right)\ [cm^2/s] & (T \geq 1443\ K) \\ \&0.005076\ \exp\left(-\frac{122780}{RT}\right)\ [cm^2/s] & (T < 1443\ K) \end{cases} \quad (8)$$

These individual fluxes are summed and normalized by the cladding circumference to define an "effective radial oxygen flux" ($J_{O,effective}$) (Eq. (9)). Here, r_o is the outer radius of cladding and $w_{path,i}$ represents the width of ZrO_2 path, which determines the effective diffusion area.

$$J_{O,effective} = \frac{1}{2\pi r_o} \sum_{i\ at\ protection\ loss} J_{O,i} w_{path,i} \quad (9)$$

This effective flux is applied as a Neumann boundary condition to the Zr matrix in TRANOX-2.0 [4]. When the surface oxygen concentration exceeds the solubility limit, the model transitions to a Dirichlet boundary condition to simulate the growth of a continuous internal ZrO_2 layer via the Stefan equation.

4.5 Integrated model

The integrated model combines the developed sub-models to simulate the complete degradation process. To account for the inherent spatial heterogeneity of coating degradation—specifically the statistical variations in Cr_2O_3 growth ($\sigma \approx 15\%$), ZrO_2 path depth ($\sigma \approx 35\%$), and width ($\sigma \approx 45\%$)—a two-step Monte Carlo sampling framework was established.

The first step captures microstructural heterogeneity by modeling the system as an aggregation of numerous discrete regions. While deterministic sub-models calculate mean kinetic values, specific parameters for each region are randomly sampled from their respective normal probability distribution functions (PDFs). This approach allows the model to effectively simulate local coating thickness non-uniformity and spatial variations in degradation rates across the cladding surface. This aggregation generates a representative curve of the overall system behavior.

The second step quantifies the propagation of sub-model uncertainties. An ensemble of 1,000 independent simulations is performed, where input kinetic constants are randomly perturbed within their validated error margins (typically ± 10–20%). The final model output is presented as the median prediction bounded by a 98% confidence interval. This rigorous probabilistic approach ensures that the model not only predicts the average failure time but also quantifies the reliability of its predictions against experimental data.

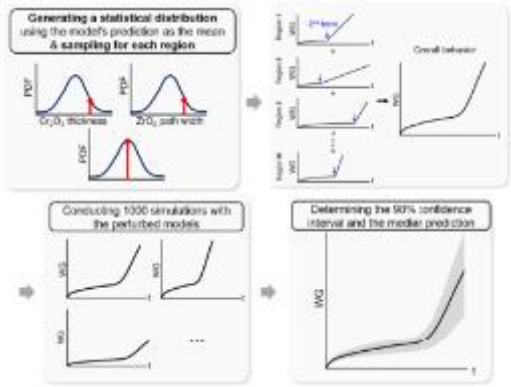

Fig. 4. Schematic of the two-step Monte Carlo uncertainty quantification framework.

The predictive performance of the integrated model was validated against experimental weight gain data (Fig. 5) and oxygen concentration profiles (Fig. 6). The model predictions show good agreement with the experimental weight gain results across the tested temperature range (1100–1300 °C). The simulation effectively captures the transition from the initial protective stage to the accelerated oxidation regime following coating failure. Furthermore, the predicted oxygen concentration profiles align well with the EPMA measurements, reproducing the oxygen diffusion depth and concentration gradient within the Zr matrix. Since the residual ductility is determined by the extent of oxygen in the Zr matrix, this accurate prediction of oxygen distribution provides a basis for the subsequent evaluation of the Ductile-to-Brittle Transition (DBT) of cladding.

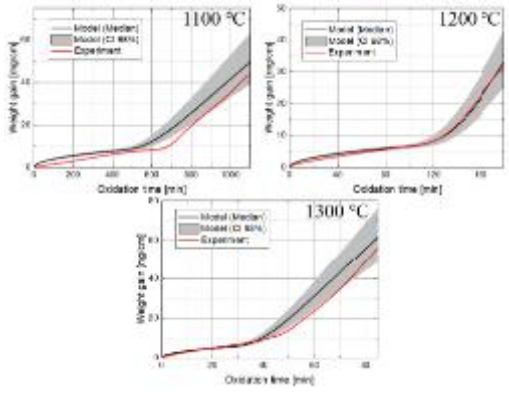

Fig. 5. Model-to-experiment comparison for oxidation weight gain at 1100–1300 °C.

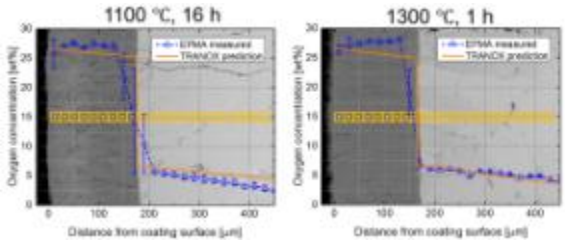

Fig. 6. Model-to-experiment comparison for oxygen distribution after being oxidized at 1100 °C for 16 h and 1300 °C for 1 h.

5. PQD results of Cr-coated cladding

5.1 Load-strain curves

Fig. 7 presents the load-strain curves of the 16 μm (AIP) Cr-coated specimens oxidized at 1200 °C for various durations (3000–9000 s) and subsequently quenched. The specimen oxidized for 3000 s exhibited significant plastic deformation without fracturing, indicating that the cladding retained sufficient ductility. However, as the oxidation time extended to 6000 s and 7500 s, the specimens showed a marked decrease in elongation, followed by sudden load drops characteristic of brittle fracture. By 9000 s, the cladding completely lost its ductility, fracturing within the elastic region. This transition highlights the rapid embrittlement induced by oxygen ingress into the Zr matrix following the loss of coating protection.

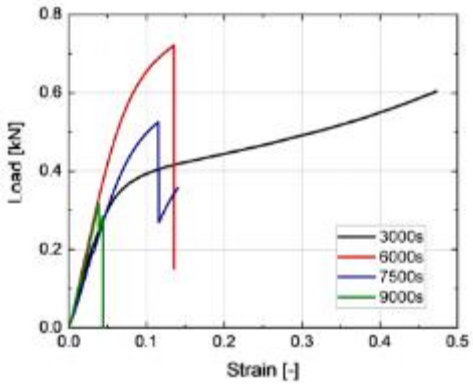

Fig. 7. Load-strain curves of the 16 μm AIP Cr-coated specimens oxidized at 1200 °C.

5.2 Predictive capability of TRANOX for DBT

The residual ductility of the cladding is governed by the thickness of the remaining ductile layer. According to established literature, for a Zr alloy to retain ductility, the layer containing an oxygen concentration below 0.7 wt% must maintain a thickness greater than 0.3 mm [7]. Fig. 8 presents the comparison between the ductile layer thickness predicted by TRANOX and the residual ductility (offset strain) derived from the experimental RCT load-strain curves. Up to approximately 6000 s of oxidation, the coating maintains its protective capability, keeping the ductile layer thickness nearly constant at its initial value. This aligns with the experimental results, where the specimens retained significant ductility well above the 2% threshold.

Beyond 6000 s, however, the loss of coating protection facilitates oxygen ingress into the matrix, leading to a rapid reduction in the ductile layer thickness. Considering the model's uncertainty range, the ductile layer thickness is predicted to fall below the critical threshold of 0.3 mm between 7720 and 8890 s, marking the onset of the DBT. Experimentally, the DBT was observed to occur between 7500 and 9000 s. The strong agreement between the predicted and observed transition times confirms that TRANOX can accurately predict the embrittlement behavior of Cr-coated cladding during accident scenarios.

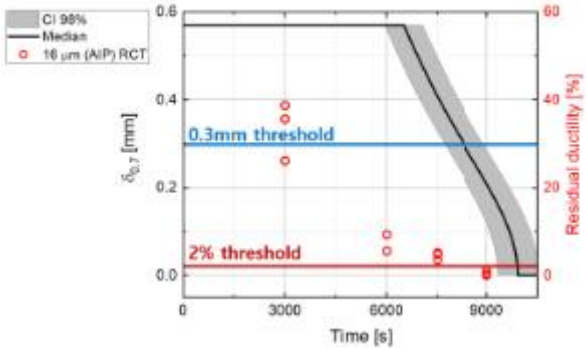

Fig. 8. Comparison of predicted ductile layer thickness and measured residual ductility at 1200 °C.

6. Conclusion

This study developed a mechanistic model to predict the protection loss and subsequent embrittlement of Cr-coated ATF under high-temperature oxidation. The model integrates sub-models for coating thinning, formation of ZrO_2 oxygen pathway, and Cr_2O_3 scale reduction and oxygen diffusion, accounting for microstructural heterogeneity through a Monte Carlo framework. Notably, the current framework can simulate the effects of local coating thickness non-uniformity and spatial variations in degradation rates. The integrated model successfully reproduced the kinetic transition to accelerated oxidation and the resulting oxygen profiles across 1100–1300 °C. PQD tests at 1200 °C confirmed a sharp embrittlement transition between 7500 and 9000 s. The model accurately predicted this DBT onset by tracking the depletion of the ductile layer, validating the framework as a reliable tool for evaluating cladding integrity.

ACKNOWLEDGEMENT

This work was supported by the Korea Institute of Energy Technology Evaluation and Planning(KETEP) and the Ministry of Climate, Energy & Environment(MCEE) of the Republic of Korea (No. RS-2022-KP002856).

REFERENCES

[1] J.-C. Brachet, E. Rouesne, J. Ribis, T. Guilbert, S. Urvoy, G. Nony, C. Toffolon-Masclet, M. Le Saux, N. Chaabane, H. Palancher, A. David, J. Bischoff, J. Augereau, and E. Pouillier, High temperature steam oxidation of chromium-coated zirconium-based alloys: Kinetics and process, Corrosion Science, Vol. 167, p. 108537, 2020.
[2] J. Deng, D. Geng, Q. Sun, Z. Song, and J. Sun, Steam oxidation of Cr-coated zirconium alloy claddings at 1200 °C: Kinetics transition and failure mechanism of Cr coatings, Journal of Nuclear Materials, Vol. 586, p. 154684, 2023.
[3] D. Kim and Y. Lee, Mechanisms of steam oxidation-induced degradation of chromium coating on zirconium alloys at high temperatures, Corrosion Science, Vol. 254, p. 113055, 2025.
[4] D. Kim, H. Yook, K. Keum, and Y. Lee, TRANOX: Model for non-isothermal steam oxidation of zircaloy cladding, Journal of Nuclear Materials, Vol. 556, p. 153153, 2021.
[5] H. Kang, D. Kim, Š. Martin, and Y. Lee, Parabolic oxidation for various chromium-coated Zr-Nb Alloy Claddings, Journal of Nuclear Materials, Vol. 615, p. 155946, 2025.
[6] D. Kim and Y. Lee, Diffusion of chromium of Cr-coated Zircaloy accident tolerant fuel cladding: Model development and experimental validation, Surface and Coatings Technology, Vol. 468, p. 129698, 2023.
[7] H. M. Chung and T. F. Kassner, Embrittlement criteria for Zircaloy fuel cladding applicable to accident situations in light-water reactors. Summary report, Argonne National Laboratory, IL, United States, 1980.